Characterising global ocean mesoscale eddy by AVISO and Haiyang-2 altimeter

International Journal of Digital Earth

ISSN: (Print) (Online) Journal homepage: www.tandfonline.com/journals/tjde20

Characterising global ocean mesoscale eddy by AVISO and Haiyang-2 altimeter

Tao Jiang, Weizeng Shao, Qingping Zou, Yongjun Jia & Xingwei Jiang

To cite this article: Tao Jiang, Weizeng Shao, Qingping Zou, Yongjun Jia & Xingwei Jiang (2024) Characterising global ocean mesoscale eddy by AVISO and Haiyang-2 altimeter, International Journal of Digital Earth, 17:1, 2347450, DOI: 10.1080/17538947.2024.2347450

To link to this article: https://doi.org/10.1080/17538947.2024.2347450

Published online: 02 May 2024.

INTERNATIONAL JOURNAL OF DIGITAL EARTH
2024, VOL. 17, NO. 1, 2347450
https://doi.org/10.1080/17538947.2024.2347450

RESEARCH LETTER

OPEN ACCESS Check for updates

Characterising global ocean mesoscale eddy by AVISO and Haiyang-2 altimeter

Tao Jiang[a], Weizeng Shao[a], Qingping Zou[b], Yongjun Jia[c] and Xingwei Jiang[c]

[a]College of Marine Sciences and Ecological Environment, Shanghai Ocean University, Shanghai, People's Republic of China; [b]Global Research Institutes, Heriot-Watt University, Edinburgh, UK; [c]National Satellite Ocean Application Service, Ministry of Natural Resources of the People's Republic of China, Beijing, People's Republic of China

ABSTRACT

This work compares the Haiyang-2 (HY-2) altimeter data with the well-recognized satellite oceanographic data (AVISO) product in the global ocean in their capability of detecting mesoscale eddy. A well-established method to detect mesoscale eddies from HY-2 and AVISO was applied to the sea level anomaly (SLA) data on a global scale in 2021−2022. It is found that the number of mesoscale eddies derived from the HY-2 dataset is three times more than that from the AVISO dataset and with larger eddy kinetic energy (EKE), shorter lifespan and smaller amplitude. Besides, the monthly-averaged number of generated and terminated mesoscale eddies is similar and the temporal variation of SLA exhibits strong lunar oscillation for both datasets. Most mesoscale eddies are generated in the mid-latitude oceans due to the Coriolis force and the strong El Niño. In the western boundary of the global ocean, equator, Antarctic Ocean and other areas with strong currents, the mesoscale eddies have stronger SLA amplitudes, EKEs and vorticity. Furthermore, EKE is low at the centre and high at the eddy meander. The spatial distribution characteristics of vorticity are the same as those of EKEs in the western boundary of oceans, but the vorticity value of HY-2 data near the equator is larger than that of AVISO data. However, considering the large detection error of eddy near the equator, no further exploration will be conducted in this paper. Furthermore, mesoscale eddies tend to move in the east–west direction due to Coriolis force and wind (Ekman transport) effects and large-scale ocean circulation or the pathway of drifters also have a certain impact. Overall, similar to AVISO data, the HY-2 data is also reliable for mesoscale identification in global oceans.

ARTICLE HISTORY
Received 25 January 2024
Accepted 19 April 2024

KEYWORDS
Mesoscale eddy; global ocean; sea level anomalies

1. Introduction

Mesoscale eddies including cyclonic eddies (CEs) and anticyclonic eddies (AEs) are the vital oceanographic driving force for sea surface height and sea surface temperature anomalies. Compared to large-scale ocean circulation, mesoscale eddies occur in a relatively small and inconspicuous range. Mesoscale-eddy generation is generally thought to be due to baroclinic and/or barotropic instability (Vallis 2006). Mesoscale eddies typically have a spatial scale of 10–100 km and a life cycle of day to months with significant kinetic energy, which play an important role in

CONTACT Weizeng Shao swz19@tsinghua.org.cn No.999, Huchenghuan Rd , Nanhui New City, Shanghai, People's Republic of China

ocean circulations, mixing and dispersion, momentum, heat and energy transport, material exchanges and ocean environment changes (Chelton et al. 2007; Dong et al. 2014; Ferrari and Wunsch 2009; Frenger et al. 2015; Martins, Hamann, and Fiúza 2002; Samelson, Schlax, and Chelton 2014; Tian et al. 2020; Wei and Wang 2023; Zhang et al. 2014). In addition, mesoscale eddies may interact with other oceanic phenomena, i.e. extreme waves generated by tropical cyclones and oceanic fronts.

For the past decades, the understanding of oceanographical dynamics relied on in-situ observations, however, detection of the mesoscale eddy manually is expensive and inefficient due to be lack of long-term observation, appropriate algorithms, high-precision data and large-scale mesoscale eddy data, *etc.* (Dickey et al. 2008; You et al. 2022). With the development of remote sensing technology and numerical models, global marine data with high spatial and temporal resolution is now available constantly, which provides an alternative robust observation of mesoscale eddies, i.e. the movement, development and spatiotemporal variations. Furthermore, synesthetic aperture radar (SAR) data (Lai et al. 2023; Shao et al. 2022) with fine spatial resolution have been used to detect mesoscale eddies over certain Arctic regions through the sea ice concentration patterns extracted from SAR (Aleskerova, Kubryakov, and Stanichny 2017; Johannessen et al. 1987). However, SAR is not capable of providing the dynamic characteristics of an eddy, i.e. vorticity and lifespan. In contrast, this information can be derived from continuous observations of altimeters over global and regional oceans. Altimeters, i.e. TOPEX/Poseidon, ERS-1/2, Jason-1/2/3, Sentinel-3 A/B, AVISO and Haiyang-2 (HY-2), have provided the sea surface height observations globally for almost 30 years by measuring the fluctuations of the sea surface relative to the geoid. The altimetry data have revealed abundant mesoscale eddies in the oceans from strong signals in the sea surface height field (Chelton et al. 2007; Pascual et al. 2006; Traon et al. 2004; Wang, Su, and Chu 2003). However, due to limited resolution, the altimetry data is not reliable for detecting mesoscale eddies with a scale about smaller than 40 kilometres (Cheng et al. 2014; Stegner et al. 2021). With fine resolution, eddies with a radius of about 20–60 kilometres may be identified from the variation of sea surface temperature induced by the vertical water mass transport, which is derived from optical image (Castellani 2006; Xia and Shen 2015).

Currently, the observed sea level anomalies (SLA) by altimeters and sea surface temperature anomalies (SSTA) by optical images are commonly used to detect mesoscale eddies. Put simply, the mesoscale eddy detection algorithm for SLA is based on physical parameters, geostrophic velocity anomalies and the combination of these two (Nencioli et al. 2010). Previous studies compared the first two methods and found that the physical parameter-based algorithm performs better than the geometric velocity field-based algorithm with high precision. Since mesoscale eddies modulate the thermal structure of the upper ocean, the SSTA-based algorithm for mesoscale eddy detection is more suitable for areas with large temperature anomalies, especially in the nearshore (Castellani 2006).

In previous studies (Karimova 2018; Tian et al. 2021), remote-sensed SLA and SSTA data were mainly used to identify mesoscale eddies, especially in the polar region (Shao et al. 2023). Although products from AVISO and HY-2 (Shao et al. 2021) altimeters are used widely to study mesoscale eddies, the differences between these two datasets are not well understood. The objective of the present study is to compare the mesoscale eddies' properties derived from the SLA measured by AVISO and HY-2 in the global ocean. The remainder of this study is arranged as follows. The remote-sensed datasets and analysis methods are introduced in Section 2. The eddy characteristics in the global ocean extracted from AVISO and HY-2 altimeters are analysed in Section 3. In Section 4, the performance of AVISO and HY-2 in measuring mesoscale eddies is further compared and discussed. The conclusions are summarised in Section 5.

2. Materials

In this section, AVISO and HY-2 datasets are described briefly. The methodology for the detection of mesoscale eddy is presented.

2.1. Altimetry data

The dataset includes the SLA data from AVISO and HY-2 from 2021 to 2022. The daily-averaged 1/4° × 1/4° gridded AVISO SLA fields, produced by the Data Unification and Altimeter Combination System/Segment Sol multi-missions d'ALTimetrie, d'orbitographie et de Localisation précise (DUACS/SSALTO) and distributed by Collecte Localis Satellites (CLS), integrate multiple satellites, i.e. ERS-1/2, Jason-1/2 and Cryosat2. The HY-2 satellite constellation, i.e. HY-2B/2C/2D, carries the altimeters for sea height measurement in the global oceans. Since 2019, HY-2 has started to release the SLA data by fusing HY-2B/2C/2D measurements. The daily-averaged SLA of HY-2 with a spatial resolution of 0.25° covers 90% of the global oceans. The example maps of the AVISO and HY-2B SLA datasets on 1 February 2022 are shown in Figure 1(a and b). Similarly, the maps of global SLA from AVISO and HY-2B on 15 July 2022 are given in Figure 1(c and d). HY-2 exhibits stronger seasonality than AVISO in the observed SLA. The Pacific Ocean, the Atlantic Ocean and the Indian Ocean, were analysed separately in this study, as highlighted by theblack rectangle in Figure 1. It is observed that the overall spatial distribution pattern of the global SLA from HY-2 and AVISO altimeters was similar although the HY-2B SLA has apparent stripes and the gradient partitioning of HY-2 SLA data is more pronounced.

2.2. Methodology

The two-dimensional sea surface current field is derived from the SLA data using the geostrophic current formula (Couvelard et al. 2012; Liu et al. 2012; Peliz, Boutov, and Teles-Machado 2013; Xu et al. 2019):

$$u = \left(\frac{\rho}{\mathrm{gf}}\right)\frac{\partial \mathrm{P}}{\partial \mathrm{y}} \tag{1}$$

$$v = \left(\frac{\rho}{\mathrm{gf}}\right)\frac{\partial \mathrm{P}}{\partial \mathrm{x}} \tag{2}$$

where

$$P = \mathrm{gh} + \mathrm{f}\sqrt{\mathrm{u}^2 + \mathrm{v}^2} \tag{3}$$

where P is the Montgomery potential based on SLA h, which is the sea surface height anomaly data; g is the gravitational acceleration constant (= 9.8 m^2/s); ρ represents the air density; u and v are the corresponding zonal and longitudinal current at latitude x and longitude y, respectively; and f is the Coriolis force constant, which is inversely proportional to the latitude. The current components derived by the above formula are applied to detect mesoscale eddies by the vector geometry algorithm. Eddy kinetic energy (EKE) is an important indicator of eddy activity intensity (Liu et al. 2022; Wang and Stefano 2023; Zhang, Chambers, and Liang 2021), given by

$$\mathrm{EKE} = \frac{1}{2}(\mathrm{u}^2 + \mathrm{v}^2) \tag{4}$$

In the identification process, the eddy centre needs to meet the following points (Nencioli et al. 2010):

1. The current component u and v have the opposite sign on either sides of the eddy centre and increases in magnitude with distance from the centre.
2. The point with the minimum velocity in the selected area is identified as the indeterminacy eddy centre.
3. Near the indeterminacy eddy centre, the rotation direction of the two adjacent velocity vectors has to be almost the same and located in the same or adjacent quadrants to ensure the same direction of rotation.

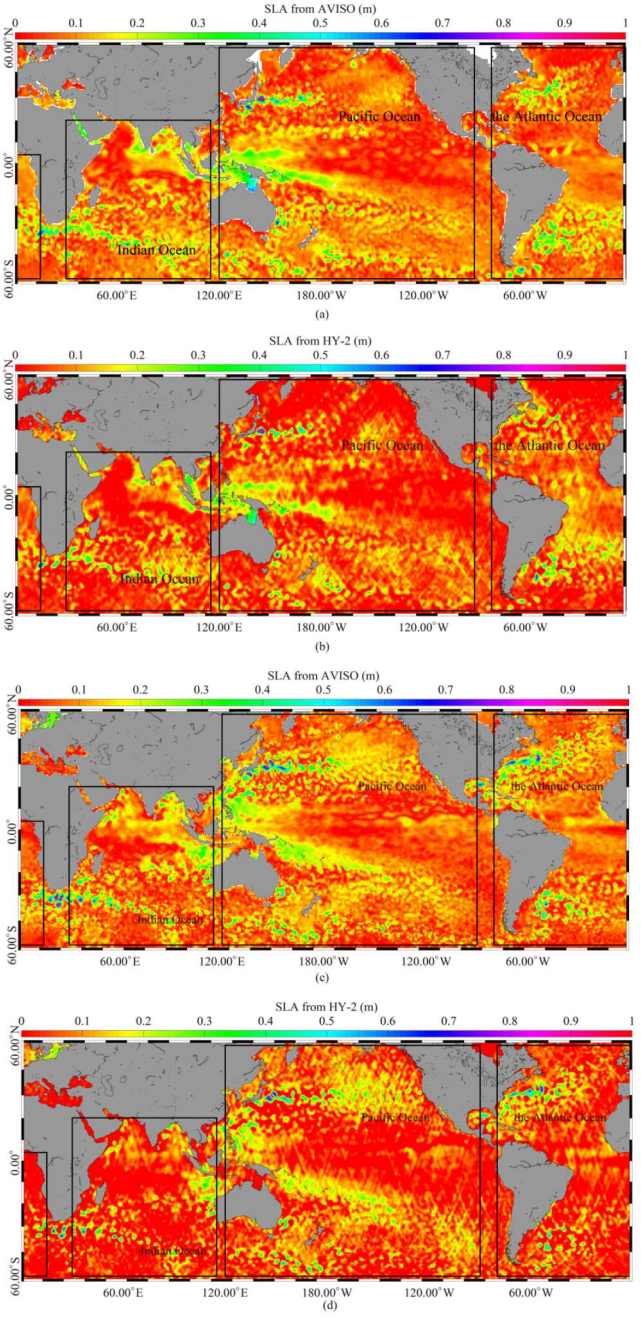

Figure 1. The global sea level anomaly (SLA) map from (a) AVISO and (b) Haiyang-2 (HY-2) on 1 February 2022 and the global SLA map from (c) AVISO and (d) Haiyang-2 (HY-2) on 15 July 2022. The black lines represent the boundary of the three oceans.

Once the eddy centre is determined, the boundary of the eddy can be calculated using the stream function that describes the streamline and the outermost closed streamline is taken as the edge of an eddy. The average distance from the eddy edge to the centre is defined as the eddy radius. Furthermore, the eddy track is described by the time evolution of the eddy centre. Although both Eulerian and the Lagrangian methods are based on the satellite-derived surface geostrophic velocities, the Lagrangian eddies are generally smaller than Eulerian eddies (Liu and Abernathey 2022). The

Eulerian methods used in this study can be biased towards erroneously detecting more eddies (Abernathey and Haller 2018; Liu et al. 2019; Tarshish et al. 2018).

3. Result

The characteristics of mesoscale eddies detected from AVISAO and HY-2 in 2021–2022, i.e. number, radius, lifespan, EKE, spatial and temporal distribution, were presented in this section.

3.1. Eddy characteristics

Mesoscale eddies within a complete lifespan were treated as one mesoscale eddy. In this study, to avoid duplicate counting, we use a trajectory tracking algorithm proposed in Doglioli et al. (2007). Within the lifespan of an eddy, the trajectory is determined through the centres and radii with the similar polarity. Figure 2 shows the eddy number, radius, lifespan and EKE of cyclonic and anticyclonic mesoscale eddies (CEs and AEs). The number, radius and lifespan of CEs are slightly greater than those of AEs based on AVISO and HY-2 datasets (Figure 2(a–c)). Interestingly, the EKEs of CEs are smaller than EKEs of AEs (Figure 2(d)). This phenomenon is more apparent for HY-2 dataset, as shown by the 10×10^{-3} m^2/s^2 EKE of CE and 11×10^{-3} m^2/s^2 EKE of AE in the Indian Ocean. The finding indicates that the current gradient of CE is smaller than that of AE over global seas.

Table 1 gives the statistics of the properties of mesoscale eddy in the three oceans, as shown in Figure 2. Overall, the differences of the four mesoscale eddy parameters between the two datasets are particularly significant. In general, compared with the results in HY-2 SLA, higher standard deviations (STDs) in radius, lifespan and amplitude except EKE are found in AVISO SLA. In other words, the properties of mesoscale eddy in AVISO have more drastic changes. The number of mesoscale eddies and the EKEs in HY-2 is greater than that in the AVISO. In the Pacific Ocean, the number in the HY-2 is three times of that in AVISO, while EKE in the HY-2 is twice times of that in AVISO in the Indian Ocean. In contrast, the radius and lifespan of mesoscale eddies detected by the HY-2 are less than that by AVISO.

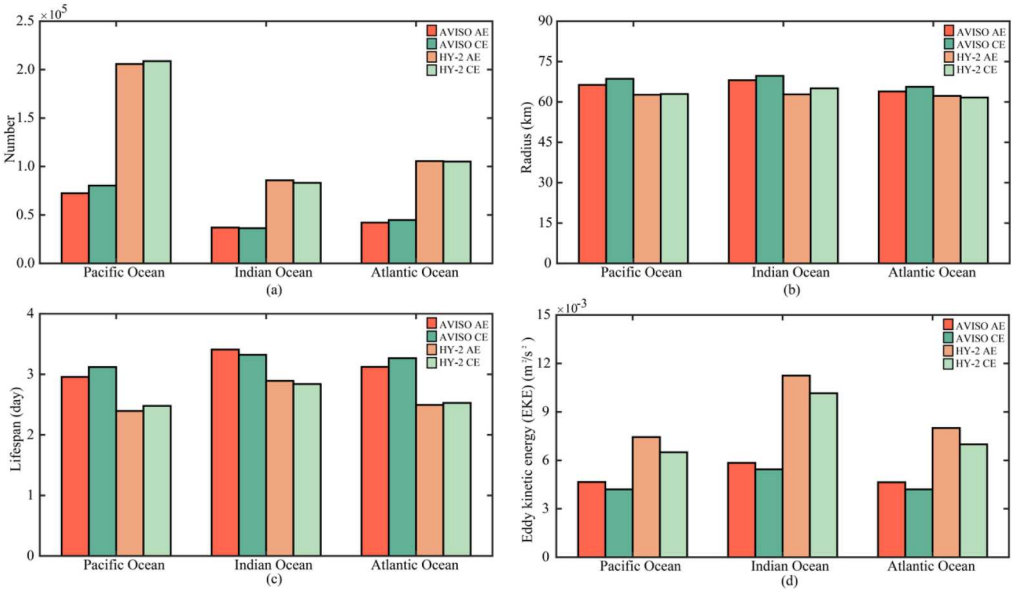

Figure 2. Comparison of (a) eddy number, (b) radius, (c) lifespan and (d) eddy kinetic energy (EKE) in three oceans detected from AVISO and HY-2. AE and CE represent anticyclonic and cyclonic eddies, respectively.

Table 1. Comparison of the HY-2 and AVISO dataset statistics in the three oceans.

		AVISO		HY-2	
Region	Parameter (unit)	CE	AE	CE	AE
Pacific Ocean	Number	84625	76392	208801	205805
	Radius (km)	68.537 (34.011)	66.377 (31.708)	62.927 (27.428)	62.681 (26.583)
	Lifespan (day)	3.3122 (5.569)	3.0425 (5.418)	2.4788 (3.296)	2.3943 (3.013)
	Amplitude (cm)	17.7586 (15.338)	17.5271 (15.534)	15.8769 (13.943)	15.4601 (13.580)
	EKE (m^2/s^2)	0.0042 (0.010)	0.0047 (0.011)	0.0065 (0.017)	0.0074 (0.022)
Indian Ocean	Number	38697	39099	83161	85712
	Radius (km)	69.764 (32.242)	67.969 (31.712)	65.062 (28.548)	62.815 (26.903)
	Lifespan (day)	3.4817 (5.834)	3.5412 (6.647)	2.8396 (3.825)	2.8915 (4.116)
	Amplitude (cm)	19.643 (15.489)	20.499 (16.599)	17.462 (14.444)	17.495 (14.691)
	EKE (m^2/s^2)	0.006 (0.011)	0.006 (0.011)	0.010 (0.031)	0.011 (0.028)
Atlantic Ocean	Number	47424	44562	105392	106089
	Radius (km)	65.597 (29.310)	63.982 (27.091)	61.569 (26.481)	62.249 (25.733)
	Lifespan (day)	3.469 (6.559)	3.057 (5.575)	2.527 (3.124)	2.494 (3.150)
	Amplitude (cm)	19.204 (16.615)	19.200 (18.227)	16.510 (14.773)	15.861 (14.647)
	EKE (m^2/s^2)	0.004 (0.009)	0.004 (0.014)	0.006 (0.021)	0.007 (0.025)

Note: Mean values (standard deviations) are shown outside (inside) the brackets.

The radii of mesoscale eddies detected by HY-2 and AVISO in the three oceans may be described by a biased normal distribution (Figure 3). The radii within 100 kilometres account for 90.36/93.61% of the total of the AVISO/HY-2. As shown in Figure 4, more short-life eddies than longer-lived eddies are observed in both AVISO and HY-2. Mesoscale eddies lasting 2 weeks account for 98% and 99% of the total of the AVISO and HY-2, respectively. This phenomenon is caused by the fact that the longer-

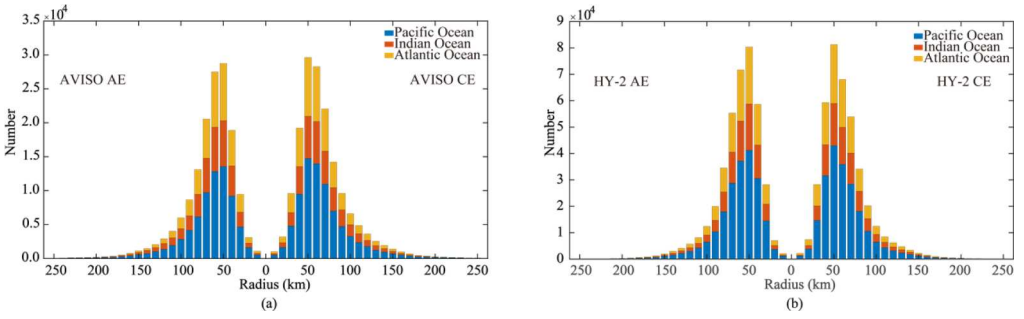

Figure 3. Histograms of eddy radii of (a) AVISO and (b) HY-2 datasets in three oceans. The left side of the coordinate axis represents AEs and the right side represents CEs.

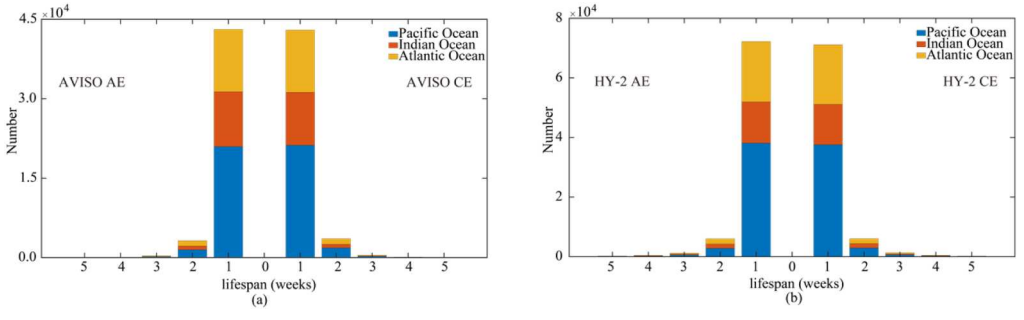

Figure 4. Histograms of eddy lifespan of (a) AVISO and (b) HY-2 datasets in three oceans. The left side of the coordinate axis represents AEs and the right side represents CEs.

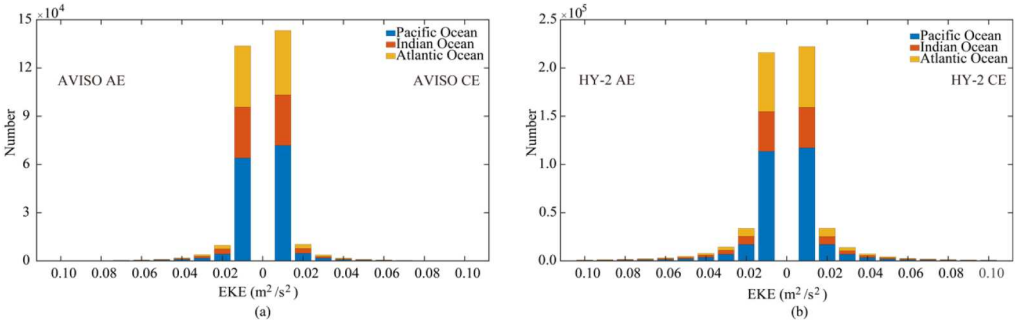

Figure 5. Histograms of eddy EKE of (a) AVISO and (b) HY-2 datasets in three oceans. The left side of the coordinate axis represents AEs and the right side represents CEs.

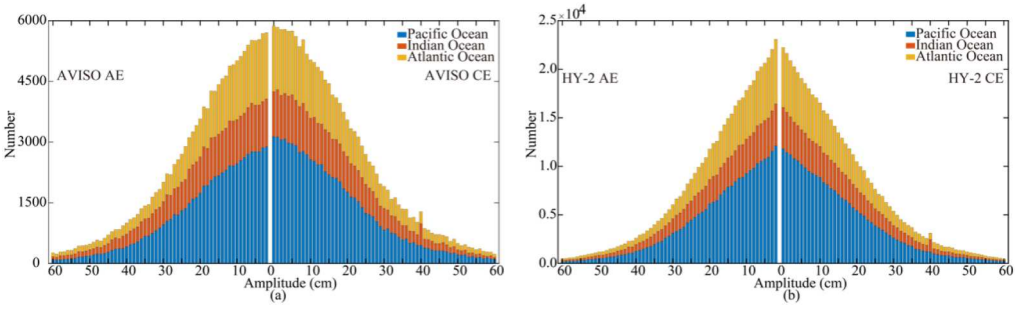

Figure 6. Histograms of eddy amplitude of (a) AVISO and (b) HY-2 datasets in three oceans. The left side of the coordinate axis represents AEs and the right side represents CEs.

lived eddies requires more energy to sustain the structure. In addition, the lifespans of 154 days derived from AVISO are significantly longer than that of 103 days from HY-2.

The spatial distribution of EKE (Figure 5) is similar to that of the lifespan shown in Figure 4. EKEs of mesoscale eddies less than 0.02 m^2/s^2 account for 99% of the total of both AVISO and HY-2. As depicted in Figure 6, histogram of amplitudes of mesoscale eddies detected by both AVISO and HY-2 obey a half-normal distribution. Moreover, the amplitudes less than 30 cm accounts for 81.63/85.64% of the total of AVISO /HY-2, which is consistent with the previous finding by You et al. (2022).

3.2. Temporal variation

The temporal variation of the monthly-averaged mesoscale eddy generation and termination number in 2021–2022 is exhibited in Figure 7. For both datasets, the number of generated and terminated CEs (AEs) is similar with a slightly difference. This behaviour is caused by the difference of lifespan in the three oceans. Besides, the generation of CEs and AEs observed by AVISO occurs the most in the Pacific Ocean and Indian Ocean and the least in the Atlantic Ocean, which ranges from 1 to 25, whereas that by HY-2 occurs most in the Pacific Ocean and least in the Indian Ocean, which ranges from 30 to 150.

The monthly-averaged radius (Figure 8) as well as EKE (Figure 9) of mesoscale eddy detected by AVISO is larger than that from HY-2 in the three oceans. The time variation

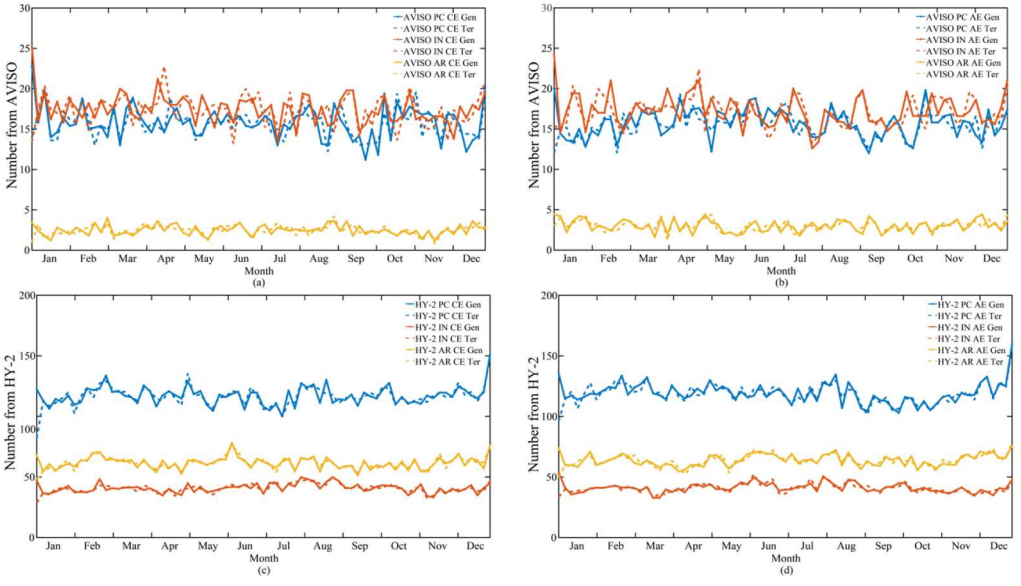

Figure 7. The temporal variation of the monthly-averaged mesoscale eddy generation and termination number in 2021–2022: (a) AVISO CEs; (b) AVISO AEs; (c) HY-2 CEs and (d) HY-2 AEs in three oceans.

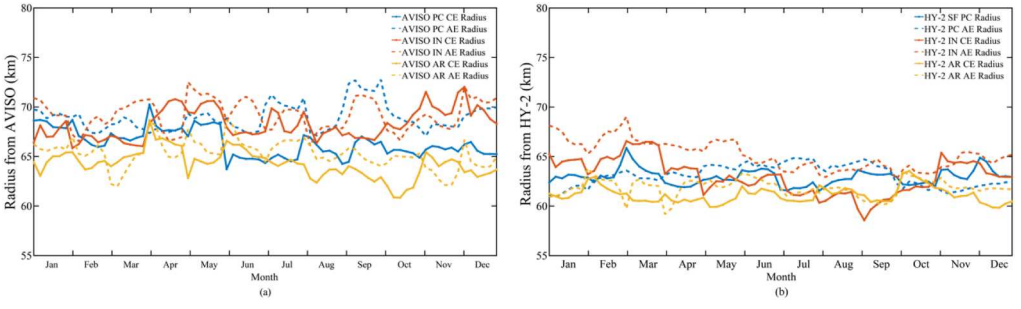

Figure 8. Temporal variation of the monthly-averaged radii of mesoscale eddies (CEs and AEs) which are detected in 2021–2022 from (a) AVISO and (b) HY-2 in three oceans.

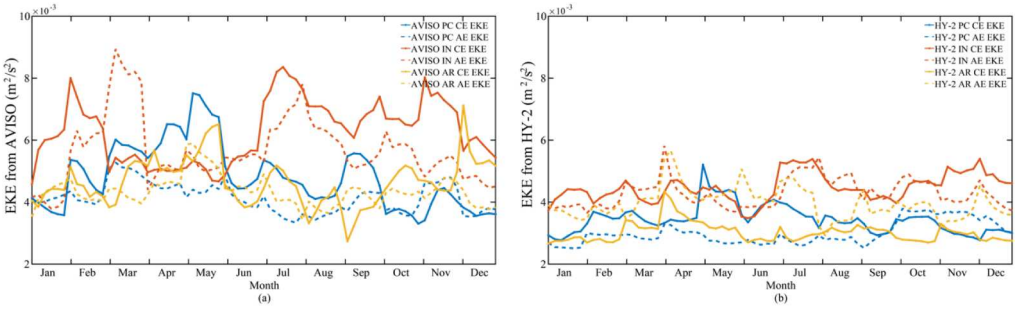

Figure 9. Temporal variation of the monthly-averaged EKEs of mesoscale eddies (CEs and AEs) detected in 2021–2022 from (a) AVISO and (b) HY-2 in three oceans.

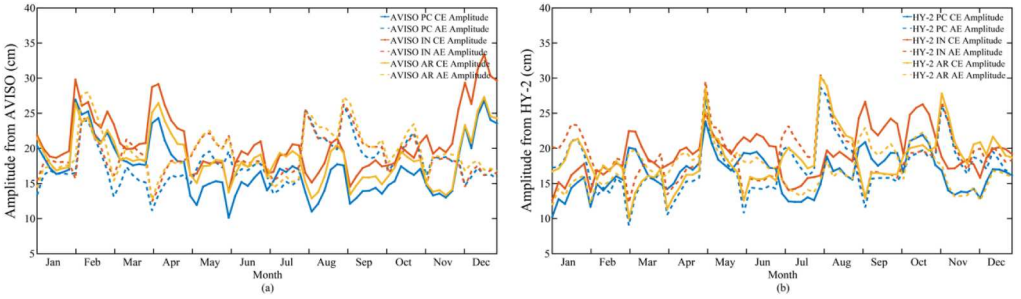

Figure 10. Temporal variation of the monthly-averaged amplitudes of mesoscale eddies (CEs and AEs) detected in 2021–2022 from (a) AVISO and (b) HY-2 in three oceans.

of the monthly-averaged amplitude of mesoscale eddy displays an obviously lunar oscillation for both datasets in three oceans within the range of 10–35 cm, as depicted in Figure 10. Besides, for both CEs and AEs of AVISO, the monthly-averaged amplitude varies consistently in three oceans. However, according to results from HY-2, this phenomenon only occurs in the Pacific Ocean and the Indian Ocean.

3.3. Spatial distribution

Here, the study area is gridded by 1.25°×1.25° rectangle. The number, radius, amplitude and EKE of the mesoscale eddy from both AVISO and HY-2 are statistically analysed on a spatial scale. For AVISO and HY-2, more mesoscale eddies are generated in the mid-latitude oceans (Figure 11), which is induced by the Coriolis force and the strong El Niño events result in enhanced sea surface height (SSH) differences and consequently stronger mean currents (Huang et al. 2023). Mesoscale eddies are usually associated with Rossby waves, which are large-scale planetary waves in the ocean. These waves can propagate westward along the equator and interact with background ocean circulation. During El Niño events, changes in atmospheric circulation can regulate the generation and propagation of Rossby waves, leading to changes in the strength and generation of mesoscale eddies. All detected eddies are grouped for a bin of 5° latitude and average values of all eddies with respect to latitude is given in Figure 12. The eddy radii increase towards the equator in the Pacific Ocean and the Atlantic Ocean, especially for AVISO.

As shown in Figure 13, it is found that large amplitudes of CEs and AEs occur in the western boundary of the Pacific Ocean and Atlantic Ocean due to the strong western boundary currents, i.e. Kuroshio and Gulf stream, which also occur in the southern hemisphere of the Indian Ocean due to the west wind drift. Similarly, large EKEs also occur in the western boundary of the Indian Ocean and near the equator of the three oceans where solar radiation is higher than other regions (Figure 14). According to the geostrophic effect, the Antarctic Circumpolar current is small than that in tropics, because the Coriolis force increases with latitude. As mentioned in previous study (Priya and Venkatesh 2024), there are many oceanic fronts in the Antarctic region. As the oceanic front encounters steep underwater terrain, it will rotate, which leads to an increase in EKE. This is probable explanation that EKE in Antarctic Ocean is strong and Western Boundary Current. Figure 15 shows the volatility of HY-2 data and AVISO data and it can be found that the HY-2 dataset shows more pronounced performance.

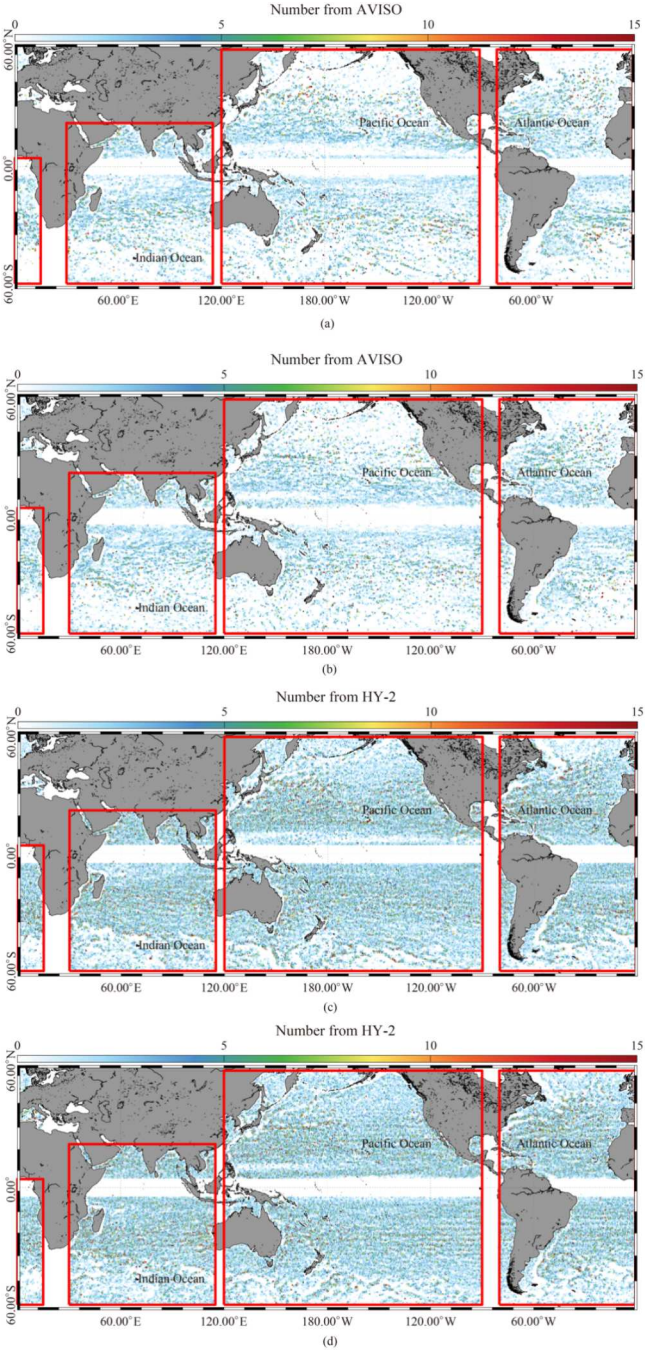

Figure 11. Number of mesoscale eddy generation. CEs and AEs detected in three oceans by the AVISO dataset are given in (a) and (b), respectively. Identically, CEs and AEs detected in three oceans by the HY-2 dataset are given in (c) and (d), respectively.

4. Discussion

To further compare the characteristics of mesoscale eddy observed from AVISO and HY-2, three cases on 1 February 2021 are selected to analyse the track, EKE and lifespan in three oceans.

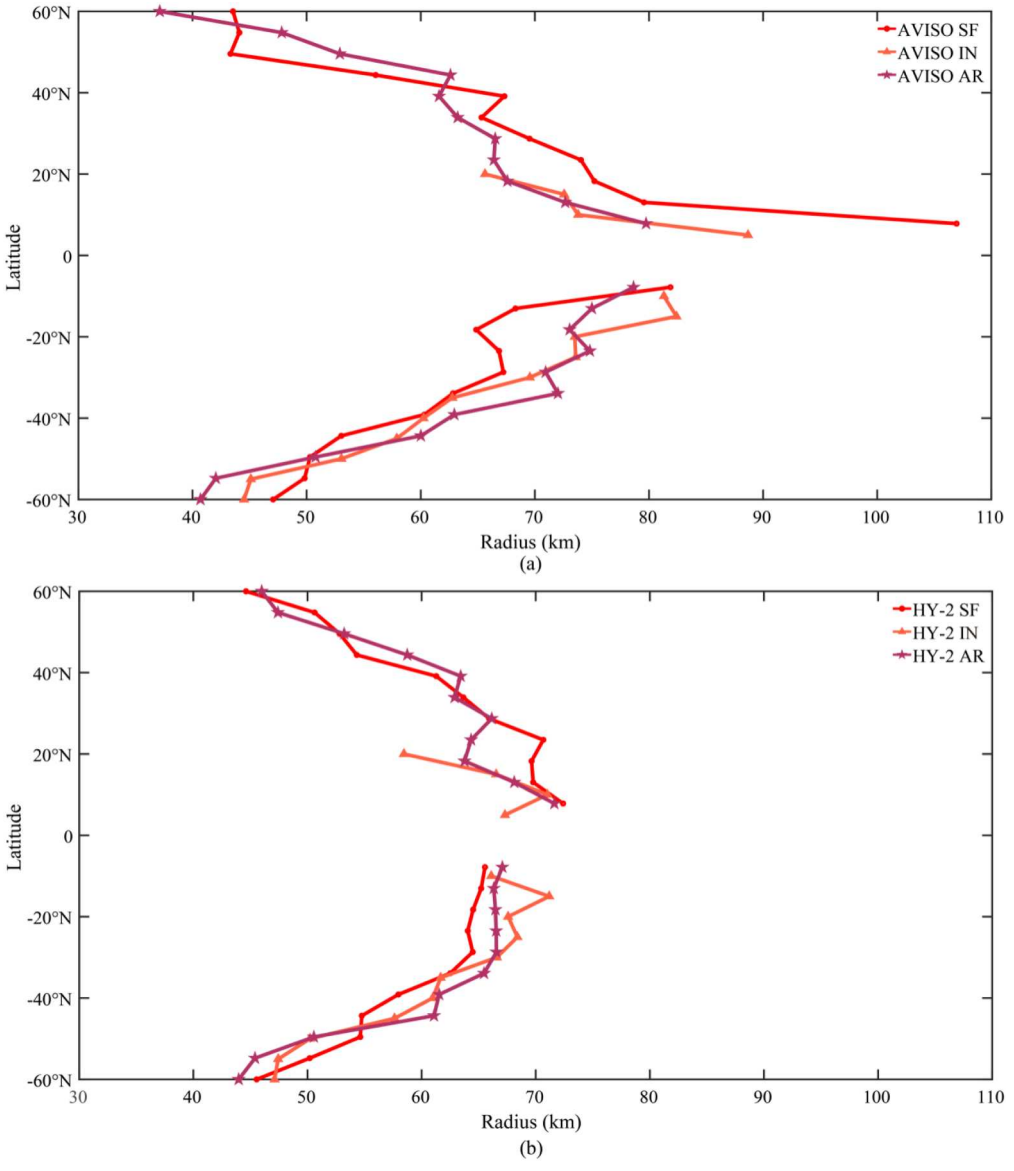

Figure 12. Distribution of radii of mesoscale eddies detected in three oceans by (a) AVISO and (b) HY-2 dataset.

Figures 16 and 17 represent CEs and AEs maps overlaid the EKE derived from HY-2 dataset, in which the lines represent the eddy meanders of high-/low-pressure regions. It is found that EKEs are low at the centres and high at the eddy meander. In addition, from the centre towards the eddy meander, the geostrophic velocity increases.

If the initial positions of two eddies identified by AVISO and HY-2 dataset are the same and the movements of two eddies are nearly consistent (i.e. along the same direction), two eddies are assumed to be a unique sample. Figure 18 shows the lifespans and tracks of CEs and AEs in three oceans extracted from the AVISO and HY-2 dataset, in which the five-pointed stars represent the geographic locations of meandering eddies. The tracks of the

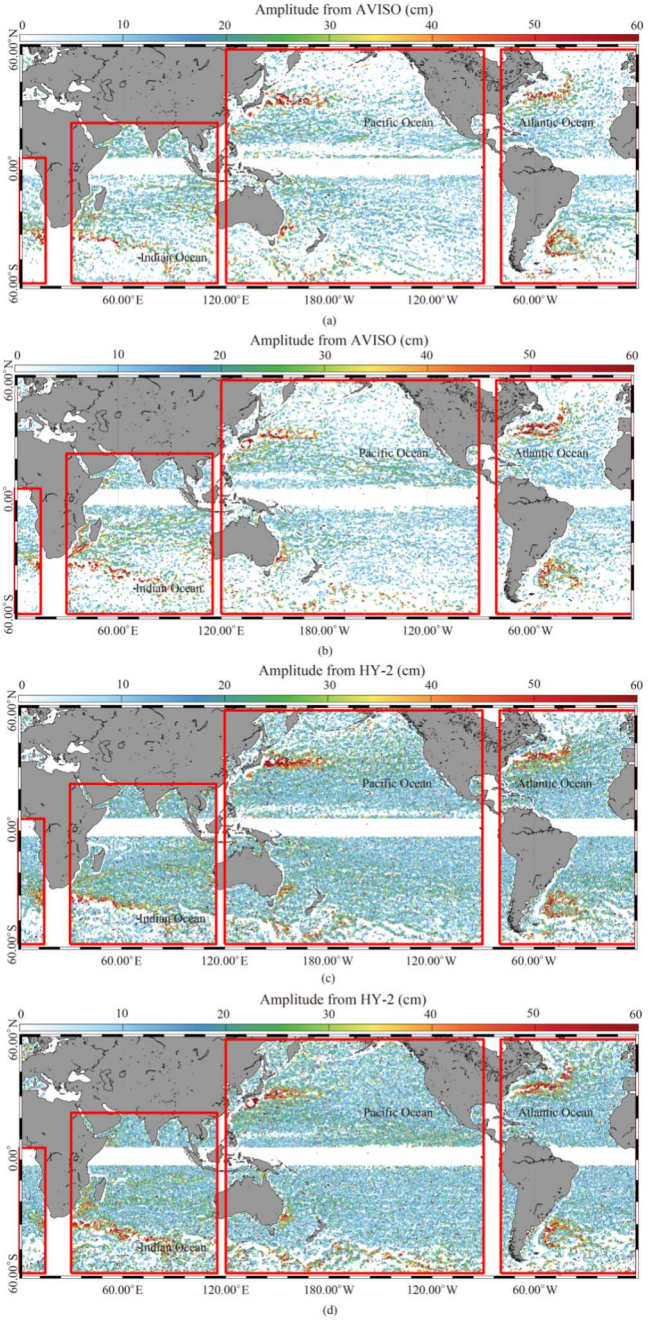

Figure 13. Distribution of amplitudes of mesoscale eddies. CEs and AEs detected in three oceans by the AVISO dataset are given in (a) and (b), respectively. Identically, CEs and AEs detected in three oceans by the HY-2 dataset are given in (c) and (d), respectively.

same mesoscale eddy detected from AVISO and HY-2 deviate due to the difference in SLA, resulting in the difference of EKE and geostrophic flow. In addition, the movement of AEs and CEs in the three oceans biases towards the east–west direction. We think the Coriolis

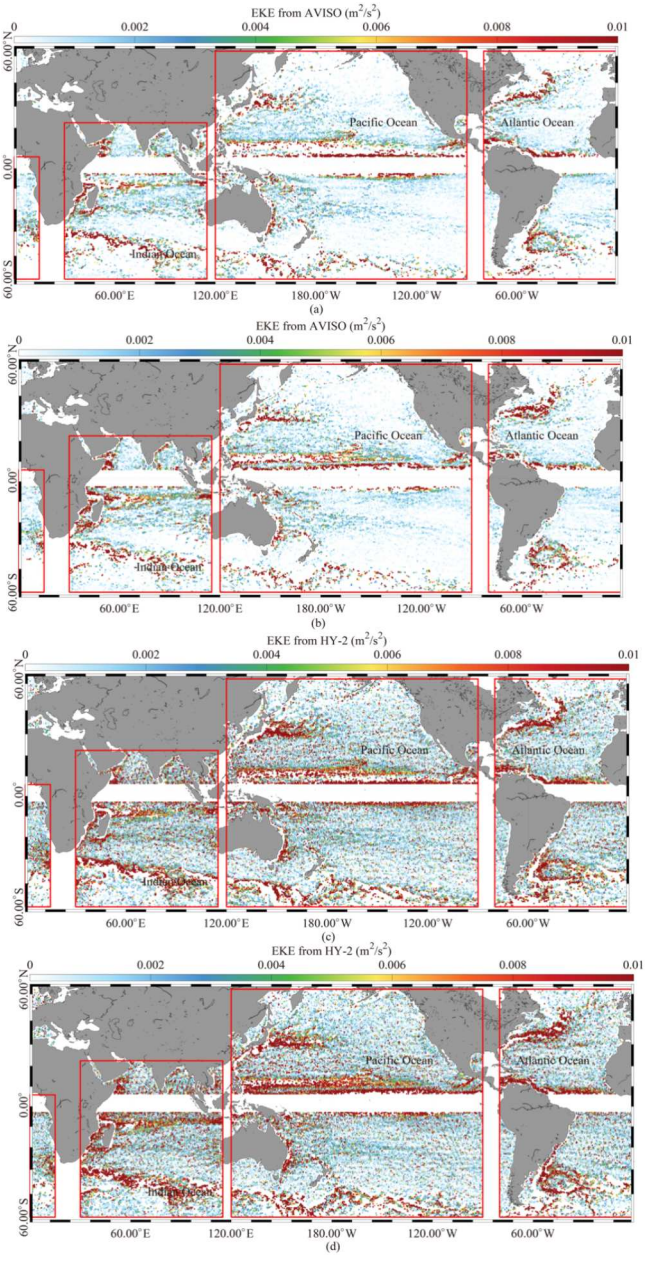

Figure 14. Distribution of EKEs of mesoscale eddies. CEs and AEs detected in three oceans by the AVISO dataset are given in (a) and (b), respectively. Identically, CEs and AEs detected in three oceans by the HY-2 dataset are given in (c) and (d), respectively.

force, large-scale ocean circulation or the pathway of drifters in the ocean (Malley et al. 2021) causes deflect along the latitude during the movement the mesoscale eddies. On the other hand, Rossby waves can transfer momentum to mesoscale eddies, thereby affecting their evolution and motion. The momentum transfer can alter the tracks and intensity of eddies,

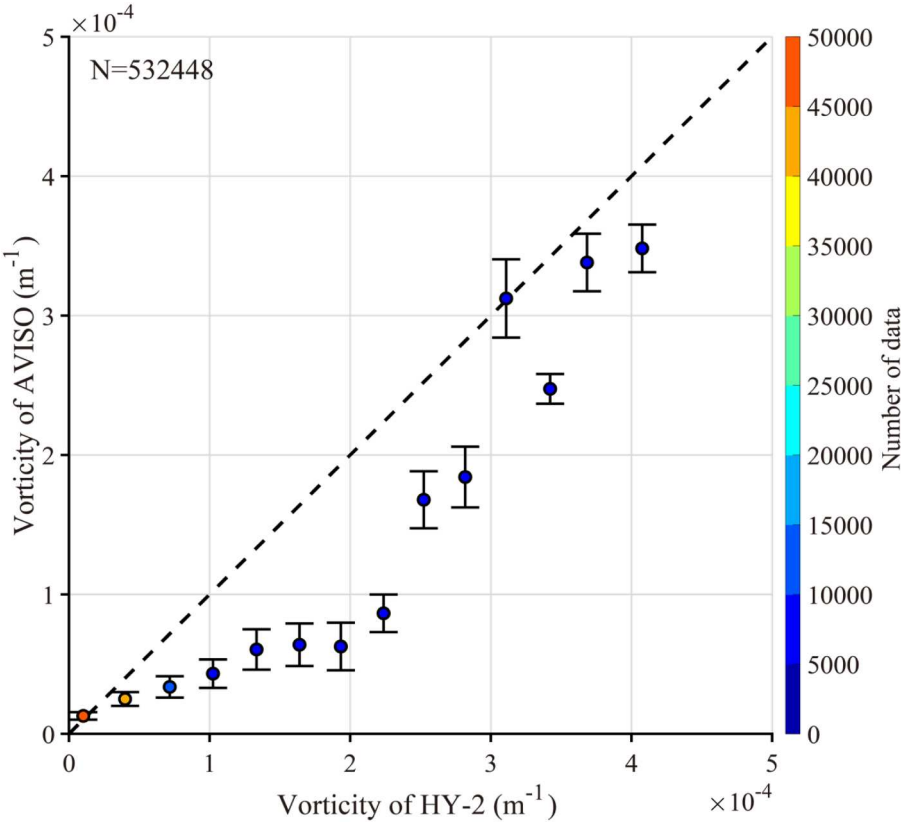

Figure 15. Distribution of vorticities of mesoscale eddies in AVISO and the HY-2 dataset.

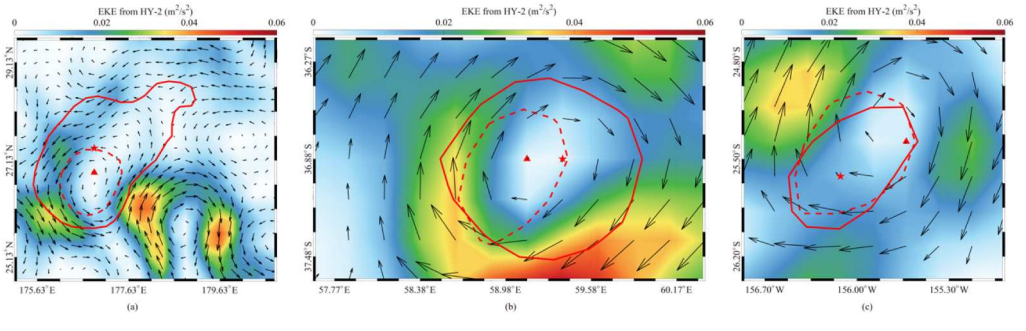

Figure 16. The certain CEs overlaid EKE derived from the HY-2 dataset on 1 February 2021 in (a) the Pacific Ocean, (b) the Indian Ocean and (c) the Atlantic Ocean. The pentagram and the triangle represent the centre of mesoscale eddy detected by AVISO and HY-2, respectively. The red solid line and dashed line represent the eddy meander of high-pressure regions in AVISO and HY-2, respectively.

resulting in an east–west trend in the eddy pathway similar to the movement of the Rossby waves (Cushman-Roisin, Chassignet, and Tang 1990; Early, Samelson, and Chelton 2011; Nof 1981).

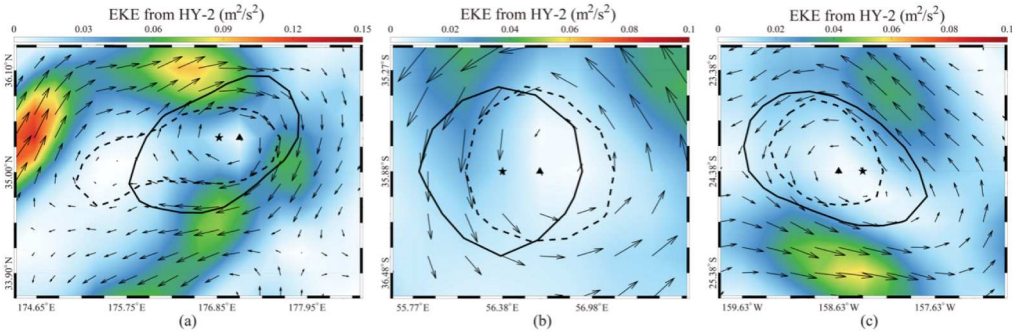

Figure 17. The certain AEs overlaid EKE derived from the HY-2 dataset on 1 February 2021 in (a) the Pacific Ocean, (b) the Indian Ocean and (c) the Atlantic Ocean. The pentagram and the triangle represent the centre of mesoscale eddy detected by AVISO and HY-2, respectively. The black solid line and dashed line represent the eddy meander of low-pressure regions in AVISO and HY-2, respectively.

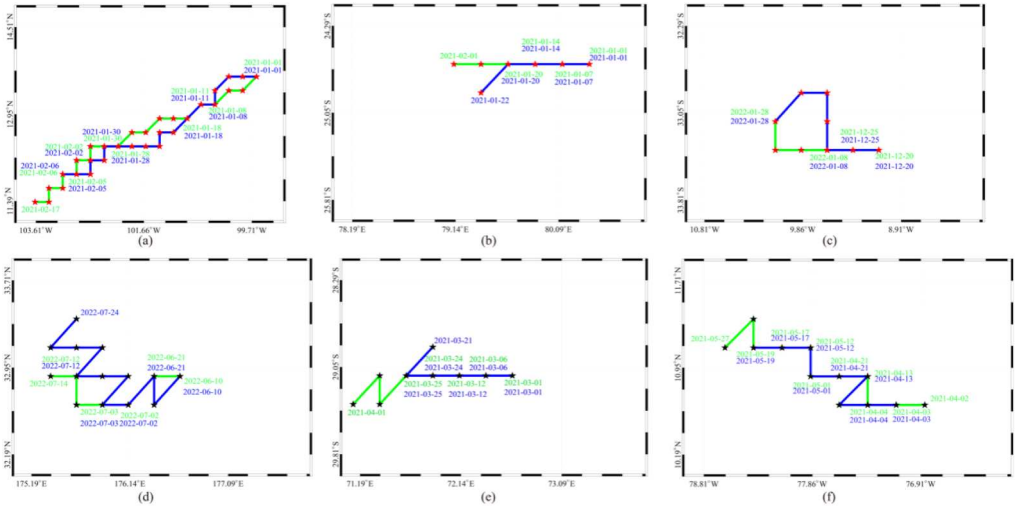

Figure 18. The tracks of the certain CEs in (a) the Pacific Ocean and (b) the Indian Ocean, (c) the Atlantic Ocean and the certain AEs in (d) the Pacific Ocean, (e) the Indian Ocean and (f) the Atlantic Ocean. The red and black pentagrams represent the CEs and AEs, respectively. The blue and green tracks of mesoscale eddy detected from HY-2 and AVISO datasets, respectively. The five-pointed stars represent the eddy centres.

5. Conclusions

The selection of an appropriate dataset is essential for the relevant research on mesoscale eddy. In this sense, to assess the capability of mesoscale eddy detection using HY-2 and AVISO datasets in the global ocean (the Pacific Ocean, the Atlantic Ocean and the Indian Ocean), the statistical analysis of characteristics of mesoscale eddy, i.e. radius, number, amplitude, EKE, temporal and spatial variation and pathway of same mesoscale eddies, is systematically conducted in 2021–2022. The following conclusions were obtained:

(1) The number, radius and lifespan for CEs are slightly greater than those from AEs detected by AVISO and HY-2 datasets, except for EKE. The AVISO dataset has a greater degree of fluctuation than that of the HY-2 dataset. The number and the EKE of HY-2 are greater than those of AVISO. In contrast, the radius and lifespan of mesoscale eddies detected by the HY-2 dataset are less than those of the AVISO dataset.

(2) The histogram of radii/amplitude of mesoscale eddy detected by AVISO and HY-2 datasets in the three oceans displays a biased normal/half-normal distribution. As for the lifespan/EKE, more short-life/low-EKE mesoscale eddies than longer-lived/large-EKE mesoscale eddies are detected by both datasets.
(3) Through the monthly-averaged analysis of mesoscale eddies in the three oceans, it is found that the number of generated and terminated CEs (AEs) is similar; however, there is a slight difference in lifespan. The amplitude of mesoscale eddy detected by AVISO and HY-2 datasets exhibits lunar oscillation within the range of 10–35 cm. More mesoscale eddies are generated in the mid-latitude ocean and this phenomenon is determined by the Coriolis force. The largest amplitude occurs in the western boundary of the Pacific Ocean and the Atlantic Ocean and the west wind drift area in the Indian Ocean. The largest EKE occurs in the western boundary, near the equator of the three oceans and around the Antarctica.
(4) Several mesoscale eddies detected simultaneously by both AVISO and HY-2 datasets are selected and EKEs are low at the centres and high at the eddy meander. The outer eddy meander of AVISO in three oceans is larger than that of HY-2. The tracks of the same mesoscale eddy observed by AVISO and HY-2 datasets do not overlap with each other completely and display different lifespans. In both datasets, AEs and CEs in the three oceans all moves biased towards the east–west direction due to Coriolis force and wind (Ekman transport), large-scale ocean circulation pattern or the pathway of drifters in the ocean (Malley et al. 2021).

In our recent work (Zhao et al. 2023), the influence of typhoon-induced wave on mesoscale eddy is preliminary investigated through a case study. In the future, the interaction between tropical cyclones (TCs) and mesoscale eddies will be investigated more in-depth through a few cases of TC passing through mesoscale eddies.

Acknowledgments

The AVISO sea level anomaly (SLA) data from multi-altimeters were provided by the Centre National d'Etudes Spatiales via https://www.aviso. altimetry.fr. In addition, SLA data from Haiyang-2 were openly downloaded from https://osdds.nsoas.org.cn.

Disclosure statement

No potential conflict of interest was reported by the author(s).

Funding

This study was partly supported by the National Natural Science Foundation of China under contract 42076238 and 42376174 and the Natural Science Foundation of Shanghai under contract 23ZR1426900.

Data availability statement

The data that support the findings of this study are available on request from the corresponding author, W.S. The data are not publicly available due to their containing information that could compromise the privacy of research participants.

References

Abernathey, R., and G. Haller. 2018. "Transport by Lagrangian Vortices in the Eastern Pacific." *American Meteorological Society* 3: 1–48. https://doi.org/10.1175/jpo-d-17-0102.1.

Aleskerova, A. A., A. A. Kubryakov, and S. V. Stanichny. 2016. "A two-Channel Method for Retrieval of the Black Sea Surface Temperature from Landsat-8 Measurements." *Izvestiya, Atmospheric and Oceanic Physics* 52 (9): 1155–1161. https://doi.org/10.1134/S0001433816090048.

Castellani, M. 2006. "Identification of Eddies from Sea Surface Temperature Maps with Neural Networks." *International Journal of Remote Sensing* 27 (8): 1601–1618. https://doi.org/10.1080/01431160500462170.

Chelton, D. B., M. G. Schlax, R. M. Samelson, and R. A. de Szoeke. 2007. "Global Observations of Large Oceanic Eddies." *Geophysical Research Letters* 34 (15): L15606. https://doi.org/10.1029/2007GL030812.

Cheng, Y. H., C. R. Ho, Q. A. Zheng, and N. J. Kuo. 2014. "Statistical Characteristics of Mesoscale Eddies in the North Pacific Derived from Satellite Altimetry." *Remote Sensing* 6 (6): 5164–5183. https://doi.org/10.3390/rs6065164.

Couvelard, X., R. M. A. Caldeira, I. B. Araujo, and R. Tome. 2012. "Wind Mediated Vorticity-Generation and Eddy-Confinement, Leeward of the Madeira Island: 2008 Numerical Case Study." *Dynamics of Atmospheres and Oceans* 58: 128–149. https://doi.org/10.1016/j.dynatmoce.2012.09.005.

Cushman-Roisin, B., E. P. Chassignet, and B. Tang. 1990. "Westward Motion of Mesoscale Eddies." *Journal of Physical Oceanography* 20 (5): 758–768. https://doi.org/10.1175/1520-0485(1990)020<0758:WMOME>2.0.CO;2.

Dickey, T. D., F. Nencioli, V. S. Kuwahara, C. Leonard, W. Black, Y. M. Rii, R. R. Bidigare, and Q. Zhang. 2008. "Physical and Bio-Optical Observations of Oceanic Cyclones West of the Island of Hawai'i." *Deep Sea Research Part II: Topical Studies in Oceanography* 55 (10-13): 1195–1217. https://doi.org/10.1016/j.dsr2.2008.01.006.

Doglioli, A. M., B. Blanke, S. Speich, and G. Lapeyre. 2007. "Tracking Coherent Structures in a Regional Ocean Model with Wavelet Analysis: Application to Cape Basin Eddies." *Journal of Geophysical Research: Oceans* 112 (C5): C05043. https://doi.org/10.1029/2006JC003952.

Dong, C. M., J. C. McWilliams, Y. Liu, and D. Chen. 2014. "Global Heat and Salt Transports by Eddy Movement." *Nature Communications* 5: 3294. https://doi.org/10.1038/ncomms4294.

Early, J. J., R. M. Samelson, and D. B. Chelton. 2011. "The Evolution and Propagation of Quasigeostrophic Ocean Eddies*." *Journal of Physical Oceanography* 41 (8): 1535–1555. https://doi.org/10.1175/2011JPO4601.1.

Ferrari, R., and C. Wunsch. 2009. "Ocean Circulation Kinetic Energy: Reservoirs, Sources, and Sinks." *Annual Review of Fluid Mechanics* 41: 253–282. https://doi.org/10.1146/annurev.fluid.40.111406.102139.

Frenger, I., M. Muennich, N. Gruber, and R. Knutti. 2015. "Southern Ocean Eddy Phenomenology." *Journal of Geophysical Research: Oceans* 120 (11): 7413–7449. https://doi.org/10.1002/2015JC011047.

Huang, M., X. Liang, Y. Yang, and Y. Zhang. 2023. "ENSO Modulates Mean Currents and Mesoscale Eddies in the Caribbean Sea." *Geophysical Research Letters* 50 (15): e2023G–L103958. https://doi.org/10.1029/2023GL103958.

Johannessen, O. M., J. A. Johannessen, E. Svendsen, R. A. Shuchman, W. J. Campbell, and E. Josberger. 1987. "Ice-Edge Eddies in the Fram Strait Marginal Ice Zone." *Science* 236 (4800): 427–429. https://doi.org/10.1126/science.236.4800.427.

Karimova, S. 2018. "Eddies in the Western Mediterranean Seen in Thermal Infrared Imagery and SLA Fields." *International Journal of Remote Sensing* 39 (13): 4304–4329. https://doi.org/10.1080/01431161.2018.1454626.

Lai, Z. Z., M. Y. Hao, W. Z. Shao, W. Shen, Y. Y. Hu, and X. W. Jiang. 2023. "Wind Field Reconstruction Based on Dual-Polarized Synthetic Aperture Radar During a Tropical Cyclone." *European Journal of Remote Sensing* 56 (1): 2273867. https://doi.org/10.1080/22797254.2023.2273867.

Le Traon, P. Y., and G. Dibarboure. 2004. "An Illustration of the Contribution of the TOPEX/Poseidon—Jason-1 Tandem Mission to Mesoscale Variability Studies." *Marine Geodesy* 27 (1-2): 3–13. https://doi.org/10.1080/01490410490489313.

Liu, T. Y., and R. Abernathey. 2023. "A Global Lagrangian Eddy Dataset Based on Satellite Altimetry." *Earth System Science Data* 15: 1765–1778. https://doi.org/10.5194/essd-15-1765-2023.

Liu, T. Y., R. Abernathey, A. Sinha, and D. Chen. 2019. "Quantifying Eulerian Eddy Leakiness in an Idealized Model." *Journal of Geophysical Research: Oceans* 124 (12): 8869–8886. https://doi.org/10.1029/2019JC015576.

Liu, Y., C. M. Dong, Y. P. Guan, D. Chen, J. McWilliams, and F. Nencioli. 2012. "Eddy Analysis in the Subtropical Zonal Band of the North Pacific Ocean." *Deep Sea Research Part I: Oceanographic Research Papers* 68: 54–67. https://doi.org/10.1016/j.dsr.2012.06.001.

Liu, Y. L., X. C. Zhang, Z. B. Sun, Z. W. Zhang, H. Sasaki, W. Zhao, and J. W. Tian. 2022. "Region-dependent Eddy Kinetic Energy Budget in the Northeastern South China Sea Revealed by Submesoscale-Permitting Simulations." *Journal of Marine Systems* 235: 103797. https://doi.org/10.1016/j.jmarsys.2022.103797.

Malley, M., A. M. Sykulski, R. Laso-Jadart, and M.-A. Madoui. 2021. "Estimating the Travel Time and the Most Likely Path from Lagrangian Drifters." *Journal of Atmospheric and Oceanic Technology* 38 (5): 1059–1073. https://doi.org/10.1175/JTECH-D-20-0134.1.

Martins, C. S., M. Hamann, and A. F. G. Fiúza. 2002. "Surface Circulation in the Eastern North Atlantic, from Drifters and Altimetry-: No. 3217." *Journal of Geophysical Research: Oceans* 107 (C12): 3217. https://doi.org/10.1029/2000jc000345.

Nencioli, F., C. M. Dong, D. Tommy, W. Libe, and C. M. James. 2010. "A Vector Geometry-Based Eddy Detection Algorithm and Its Application to a High-Resolution Numerical Model Product and High-Frequency Radar Surface Velocities in the Southern California Bight." *Journal of Atmospheric and Oceanic Technology* 27 (3): 564–579. https://doi.org/10.1175/2009JTECHO725.1.

Nof, D. 1981. "On the β-Induced Movement of Isolated Baroclinic Eddies." *Journal of Physical Oceanography* 11 (12): 1662–1672. https://doi.org/10.1175/1520-0485(1981)011<1662:OTIMOI>2.0.CO;2.

Pascual, A., Y. Faugère, G. Larnicol, and P. Y. le Traon. 2006. "Improved Description of the Ocean Mesoscale Variability by Combining Four Satellite Altimeters." *Geophysical Research Letters* 33: L02611. https://doi.org/10.1029/2005GL024633.

Peliz, A., D. Boutov, and A. Teles-Machado. 2013. "The Alboran Sea Mesoscale in a Long Term High Resolution Simulation: Statistical Analysis." *Ocean Modelling* 72: 32–52. https://doi.org/10.1016/j.ocemod.2013.07.002.

Priya, M. G., and K. Venkatesh. 2024. "Exploring the Frozen Frontier: Unmanned Aerial Vehicles and Multispectral Sensors Unveiling Cryosphere Dynamics in East Antarctica's Dronning Maud Land." *GIScience & Remote Sensing* 61 (3): 2302739. https://doi.org/10.1080/15481603.2024.2302739.

Samelson, R. M., M. G. Schlax, and D. B. Chelton. 2014. "CORRIGENDUM." *Journal of Physical Oceanography* 44 (9): 2588–2589. https://doi.org/10.1175/JPO-D-14-0139.1.

Shao, W. Z., B. Y. Duan, Y. Y. Hu, J. C. Zuo, and X. W. Jiang. 2023. "Analysis of Mesoscale Eddy in the Nordic Seas and Barents Sea Using Multi-Satellite Data." *Journal of Sea Research* 196 (12): 102443. https://doi.org/10.1016/j.seares.2023.102443.

Shao, W. Z., T. Jiang, X. W. Jiang, Y. G. Zhang, and W. Zhou. 2021. "Evaluation of Sea Surface Winds and Waves Retrieved from the Chinese HY-2B Data." *IEEE Journal of Selected Topics in Applied Earth Observations and Remote Sensing* 14 (10): 9624–9635. https://doi.org/10.1109/JSTARS.2021.3112760.

Shao, W. Z., X. W. Jiang, Z. F. Sun, Y. Y. Hu, A. Marino, and Y. G. Zhang. 2022. "Evaluation of Wave Retrieval for Chinese Gaofen-3 Synthetic Aperture Radar." *Geo-spatial Information Science* 25 (2): 229–243. https://doi.org/10.1080/10095020.2021.2012531.

Stegner, A., B. le Vu, F. Dumas, M. A. Ghannami, A. Nicolle, C. Durand, and Y. Faugere. 2021. "Cyclone-Anticyclone Asymmetry of Eddy Detection on Gridded Altimetry Product in the Mediterranean Sea." *Journal of Geophysical Research: Oceans* 126 (9): e2021JC017475. https://doi.org/10.1029/2021JC017475.

Tarshish, N., R. Abernathey, C. Zhang, O. D. Carolina, I. F. Griffies, and G. M. Stephen. 2018. "Identifying Lagrangian Coherent Vortices in a Mesoscale Ocean Model." *Ocean Modelling* 130 (7): 15–28. https://doi.org/10.1016/j.ocemod.2018.07.001.

Tian, F. L., Z. J. Li, Z. H. Yuan, and G. Chen. 2021. "Eddygraph: The Tracking of Mesoscale Eddy Splitting and Merging Events in the Northwest Pacific Ocean." *Remote Sensing* 13 (17): 3435. https://doi.org/10.3390/rs13173435.

Tian, F. L., D. Wu, L. M. Yuan, and G. Chen. 2020. "Impacts of the Efficiencies of Identification and Tracking Algorithms on the Statistical Properties of Global Mesoscale Eddies Using Merged Altimeter Data." *International Journal of Remote Sensing* 41 (8): 2835–2860. https://doi.org/10.1080/01431161.2019.1694724.

Vallis, G. K. 2006. *Atmospheric and Oceanic Fluid Dynamics: Fundamentals and Large-Scale Circulation*. (2nd ed. Falmouth, UK: Cambridge University Press.

Wang, Q., and P. Stefano. 2023. "Causal Forcing Analysis on the Low-Frequency Variations of Eddy Kinetic Energy in the Kuroshio Extension Region." *Journal of Climate* 36 (11): 3749–3763. https://doi.org/10.1175/JCLI-D-22-0702.1.

Wang, G. H., J. L. Su, and P. C. Chu. 2003. "Mesoscale Eddies in the South China Sea Observed with Altimeter Data." *Geophysical Research Letters* 30 (21): 2121. https://doi.org/10.1029/2003gl018532.

Wei, L. S., and C. Z. Wang. 2023. "Characteristics of Ocean Mesoscale Eddies in the Agulhas and Tasman Leakage Regions from Two Eddy Datasets." *Deep Sea Research Part II: Topical Studies in Oceanography* 208 (13): 105264. https://doi.org/10.1016/j.dsr2.2023.105264.

Xia, Q., and H. Shen. 2015. "Automatic Detection of Oceanic Mesoscale Eddies in the South China Sea." *Chinese Journal of Oceanology and Limnology* 33 (5): 1334–1348. https://doi.org/10.1007/s00343-015-4354-9.

Xu, G. J., C. Cheng, W. X. Yang, W. H. Xie, L. M. Kong, R. L. Hang, F. R. Ma, C. M. Dong, and J. S. Yang. 2019. "Oceanic Eddy Identification Using an AI Scheme." *Remote Sensing* 11 (11): 1349. https://doi.org/10.3390/rs11111349.

You, Z. W., L. X. Liu, B. J. Bethel, and C. M. Dong. 2022. "Feature Comparison of Two Mesoscale Eddy Datasets Based on Satellite Altimeter Data." *Remote Sensing* 14 (1): 116. https://doi.org/10.3390/rs14010116.

Zhang, Y., D. Chambers, and X. F. Liang. 2021. "Regional Trends in Southern Ocean Eddy Kinetic Energy." *Journal of Geophysical Research: Oceans* 126 (6): e2020JC016973. https://doi.org/10.1029/2020JC016973.

Zhang, C. H., X. L. Xi, S. T. Liu, L. J. Shao, and X. H. Hu. 2014. "A Mesoscale Eddy Detection Method of Specific Intensity and Scale from SSH Image in the South China Sea and the Northwest Pacific." *Science China Earth Sciences* 57 (8): 1897–1906. https://doi.org/10.1007/s11430-014-4839-y.

Zhao, Z., J. Shi, W. Z. Shao, R. Yao, and H. Li. 2023. "The Influence of Typhoon-Induced Wave on the Mesoscale Eddy." *Atmosphere* 14 (12): 1804. https://doi.org/10.3390/atmos14121804.